



HAL
open science

Tunable corrugated patterns in an active nematic sheet

Anis Senoussi, Shunnichi Kashida, Raphaël Voituriez, Jean-Christophe Galas,
Ananyo Maitra, André Estévez-Torres

► **To cite this version:**

Anis Senoussi, Shunnichi Kashida, Raphaël Voituriez, Jean-Christophe Galas, Ananyo Maitra, et al.. Tunable corrugated patterns in an active nematic sheet. Proceedings of the National Academy of Sciences of the United States of America, 2019, pp.201912223. 10.1073/pnas.1912223116 . hal-02334253

HAL Id: hal-02334253

<https://hal.science/hal-02334253>

Submitted on 27 Nov 2019

HAL is a multi-disciplinary open access archive for the deposit and dissemination of scientific research documents, whether they are published or not. The documents may come from teaching and research institutions in France or abroad, or from public or private research centers.

L'archive ouverte pluridisciplinaire **HAL**, est destinée au dépôt et à la diffusion de documents scientifiques de niveau recherche, publiés ou non, émanant des établissements d'enseignement et de recherche français ou étrangers, des laboratoires publics ou privés.

Tunable corrugated patterns in an active nematic sheet

Anis Senoussi,[†] Shunnichi Kashida,[†] Raphael Voituriez,^{†,‡} Jean-Christophe Galas,^{*,†} Ananyo Maitra,^{*,†} and André Estevez-Torres^{*,†}

¹

[†]*Sorbonne Université and CNRS, Laboratoire Jean Perrin, F-75005, Paris, France*

[‡]*Sorbonne Université and CNRS, Laboratoire de Physique Théorique de la Matière Condensée, F-75005, Paris, France*

E-mail: jean-christophe.galas@upmc.fr; nyomaitra07@gmail.com; andre.estevez-torres@upmc.fr

2 **Abstract**

3 Active matter locally converts chemical energy into mechanical work and, for this
4 reason, it provides new mechanisms of pattern formation. In particular, active nematic
5 fluids made of protein motors and filaments are far-from-equilibrium systems that may
6 exhibit spontaneous motion, leading to actively-driven spatio-temporally chaotic states
7 in two and three dimensions and coherent flows in three dimensions (3D). Although
8 these dynamic flows reveal a characteristic length scale resulting from the interplay
9 between active forcing and passive restoring forces, the observation of static and large
10 scale spatial patterns in active nematic fluids has remained elusive. In this work, we
11 demonstrate that a 3D solution of kinesin motors and microtubule filaments sponta-
12 neously forms a 2D free-standing nematic active sheet that actively buckles out-of-plane
13 into a centimeter-sized periodic corrugated sheet that is stable for several days at low
14 activity. Importantly, the nematic orientational field does not display topological de-
15 fects in the corrugated state and the wavelength and stability of the corrugations are
16 controlled by the motor concentration, in agreement with a hydrodynamic theory. At
17 higher activities these patterns are transient and chaotic flows are observed at longer
18 times. Our results underline the importance of both passive and active forces in shap-
19 ing active matter and demonstrate that a spontaneously-flowing active fluid can be
20 sculpted into a static material through an active mechanism.

21 **Significance:** To what extent can we engineer matter that shapes itself? To investigate
22 this question we study an aqueous solution containing molecular motors that walk on protein
23 filaments. When the filaments are long and attract each other, bundles of filaments are
24 parallelly oriented. We show that such a nematic solution in the presence of multimers
25 of motors has an unexpected behavior: it forms a fluid film that autonomously wrinkles.
26 The observed wrinkles have a well-defined wavelength that decreases with increasing motor
27 concentration. The wrinkles are either stable or break into a chaotic flowing state at high
28 motor concentration, providing insights into how to engineer static or dynamic materials
29 with this class of active matter.

30 Active matter is composed of subunits that convert free energy into mechanical work.
31 It comprises systems composed of objects with very different sizes, from flocks of animals¹
32 and bacterial colonies² to gels of cytoskeletal proteins.^{3,4} Active matter has attracted much
33 attention, both theoretically and experimentally, because it displays phase transitions and
34 states that greatly differ from those observed at equilibrium, such as motile ordered states and
35 spontaneous coherent or incoherent flow.⁵⁻⁹ Among the active systems that can be studied
36 in the laboratory, those composed of the protein filaments and motors that constitute the
37 cytoskeleton of the eukaryotic cell are of special interest for three reasons: i) their biological
38 importance,^{10,11} ii) the possibility to make purified systems that can be easily controlled and
39 studied,^{3,4,12} and iii) their potential to make self-organising materials.¹³

40 Depending on the conditions, cytoskeletal active systems display a wide array of dynamic
41 behaviors. Isotropic systems contract^{12,14-16} and buckle¹⁷ in three dimensions (3D). Polar
42 ones generate density waves¹⁸ and large scale vortices¹⁹ in 2D, and asters and vortices³ in
43 3D. Nematic systems display spatio-temporally chaotic flows both in 2D^{4,20,21} and in 3D,^{4,22}
44 and also coherent flow²² in 3D. This diversity of behaviors is qualitatively understood by a
45 hydrodynamic theory.⁵⁻⁹ However, we currently do not fully understand why one behavior
46 is observed in a given experimental system and not in another and which experimental
47 parameter has to be modified to switch from one state to another. This is due, on the one
48 hand, to the difficulty of measuring the phenomenological parameters of the hydrodynamic
49 theory and, on the other hand, to the use of two experimental systems, actin/myosin and
50 microtubule/kinesin, with very different microscopic properties. In this regard, the recent
51 demonstration that global contractions^{12,15} and chaotic flows in 2D^{4,21} were present in both
52 systems, and the understanding of the nematic to polar transition in microtubule/kinesin
53 systems²³ has clarified the design of these dynamic behaviors. Yet, the two aforementioned
54 difficulties remain, hindering the development of controllable active materials.

55 In this work, we report the observation of a novel static patterned state in an active
56 nematic fluid, we provide a semi-quantitative interpretation to why this state is observed and

57 we show which experimental parameters need to be tuned to reach either this static state or
58 a previously-reported flow state. More precisely, we demonstrate that a microtubule/kinesin
59 nematic fluid that is known to flow in 3D^{4,22} can be rationally engineered to form a thin
60 static corrugated sheet in three dimensions, a behavior that has only recently been observed
61 in isotropic and cross-linked actin/myosin gels¹⁷ that cannot flow. Essentially, the fluid
62 contracts anisotropically along its two shortest dimensions to form a thin sheet of gel that
63 freely floats in the aqueous solution, mainly due to passive depletion forces. Simultaneously,
64 the extensile active stress generated by the motors buckles the sheet along the direction
65 perpendicular to its plane, forming a corrugated sheet of filaments with a well-controlled
66 wavelength of the order of 100 μm over an area of 10 mm^2 . We demonstrate that this out-of-
67 plane buckling differs both from classical Euler buckling in passive gels^{24,25} and from the flow-
68 generating in-plane buckling that is common in 2D active nematic gels.^{4,22,26,27} Importantly,
69 nematic topological defects are not observed and we provide a theoretical prediction of the
70 dependence of the wavelength with the motor concentration and with the thickness of the
71 fluid that is in agreement with the experiments. Finally, we show that the transition between
72 static corrugations and chaotic flow can be experimentally controlled by two parameters, the
73 motor concentration and the attractive interactions between microtubule filaments.

74 **Results and Discussion**

75 **A 3D active nematic fluid forms a static corrugated sheet**

76 The active fluid is constituted of a dense suspension of non-growing microtubules bundled
77 together by a depletion agent and by clusters of kinesin-1 motors (Figure 1a). We use the
78 word fluid, instead of gel, to underline the fact that the system does not present irreversible
79 crosslinks, as actin gels do.¹⁷ It is supplemented with ATP and an ATP-regeneration system
80 that drives the system out of equilibrium by keeping the motor active for at least 4 h.
81 Additionally, the microtubule bundles are fluorescent because they bear a small fraction of

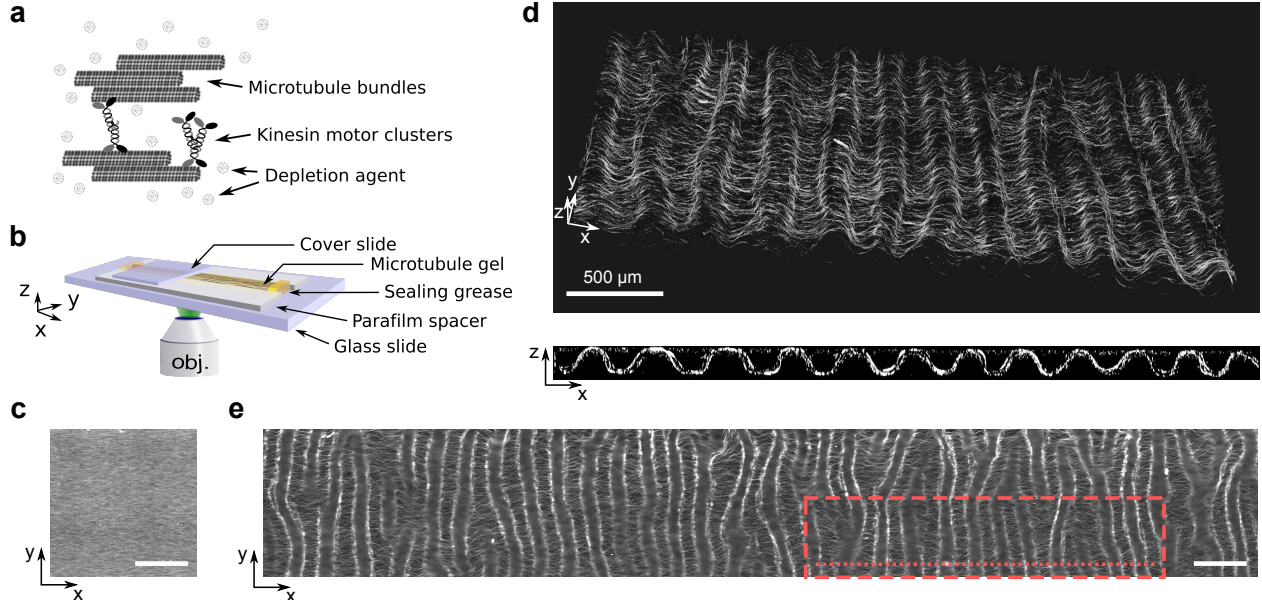


Figure 1: At low motor concentration a 3D active nematic fluid creates a thin corrugated sheet of well defined wavelength. **a** Scheme of the components of the active fluid formed by non-growing microtubules bundled together by a depletion agent and clusters of kinesin motors. **b** Scheme of the channel where the fluid (in yellow) is observed. **c** Epifluorescence image of the fluid at initial time. **d** Confocal images in 3D (top) and cross-section in the xz plane (bottom) of the fluid after 300 min. **e** Epi-fluorescence image of the same sample after one day and over a $9.5 \times 1.4 \text{ mm}^2$ area, the red dashed rectangle and the red dotted line respectively indicate the region where the top and bottom images in panel d were recorded. Scale bars are $500 \mu\text{m}$ and motor concentration 0.5 nM .

82 fluorescent tubulin, allowing their observation by fluorescence microscopy. This system is
 83 similar to previously published active nematic fluids⁴ but it differs in several important ways:
 84 the microtubules are longer ($8 \pm 6 \mu\text{m}$ instead of $1 \mu\text{m}$, Figure S1), the kinesin used here,²⁸
 85 K430, is different from the standard K401 (it comes from a different organism and forms
 86 non-specific clusters), and its typical concentration is two orders of magnitude lower (see SI
 87 Section 1). The active fluid is prepared inside a long and shallow channel of rectangular
 88 cross-section, with length $L = 22 \text{ mm}$, width $W = 1.5 \text{ mm}$ and height $H = 0.13 \text{ mm}$ (see SI
 89 Methods). Initially, the density of microtubule bundles is homogeneous in 3D but they are
 90 aligned along the long axis of the channel, parallel to x (Figure 1b-c). This nematic order
 91 arises spontaneously during the filling process of the channel by capillarity, the angle of the
 92 director of the nematic with the x axis being $2 \pm 16^\circ$ (Figure S2).

93 In the presence of 0.5 nM of motors, confocal images recorded after 300 min show that
 94 the active fluid has contracted along z and buckled in the xz plane to form a corrugated sheet
 95 whose hills and valleys reach the top and bottom walls of the channel and whose grooves are
 96 strikingly parallel to the y axis (Figure 1d). The thickness of the sheet is $\ell_z = 35 \pm 5 \mu\text{m}$ and
 97 the wavelength of the corrugations is $\lambda = 285 \pm 15 \mu\text{m}$. This periodic pattern extends along an
 98 area of at least $9.5 \times 1.4 \text{ mm}^2$, with dislocations corresponding to the junction of two valleys
 99 or hills. Notably, these dislocations in the periodic undulatory pattern do not correspond to
 100 defects in the nematic field. The pattern can also be visualized in epifluorescence, where it
 101 appears in the form of focused and defocused bands (Figure 1e).

102 **During the formation of the corrugations the fluid buckles along z**
 103 **and contracts along z and y**

104 To elucidate the mechanism of pattern formation we recorded confocal (Movie S1) and
 105 epifluorescence time-lapse images of a buckling fluid at 0.5 nM motors (Figure 2). Two
 106 processes are observed: buckling along the z direction and contraction along z and y . These
 107 processes are quantified by the angle ϕ between the microtubule bundles and the x axis in
 108 the xz plane, and by $\Delta\ell_z$ and $\Delta\ell_y$, the contracted lengths of the fluid along the z and y
 109 axes, respectively. Buckling initially proceeds at a rate $\omega_\phi = 0.3 \text{ min}^{-1}$ but later slows down
 110 until reaching a maximal buckling angle $\phi^{max} = 32.2 \pm 0.5^\circ$ (Figure 2c) and an amplitude
 111 $h^{max} = 22 \pm 3 \mu\text{m}$ after 100 min. Contraction along z and y is significantly slower with onset
 112 rates $\omega_z = 6.4 \times 10^{-2} \text{ min}^{-1}$ and $\omega_y = 1.5 \times 10^{-2} \text{ min}^{-1}$, respectively, to reach maximum
 113 amplitudes $\Delta\ell_z^{max} = 40 \mu\text{m}$ and $\Delta\ell_y^{max} = 210 \mu\text{m}$ (Figure 2d). Note that the relative
 114 contraction amplitudes $\Delta\ell_z^{max}/H = 0.40$ and $\Delta\ell_y^{max}/W = 0.14$ are significantly different,
 115 indicating that the final contracted state does not correspond to a nematic liquid droplet at
 116 equilibrium.²⁹

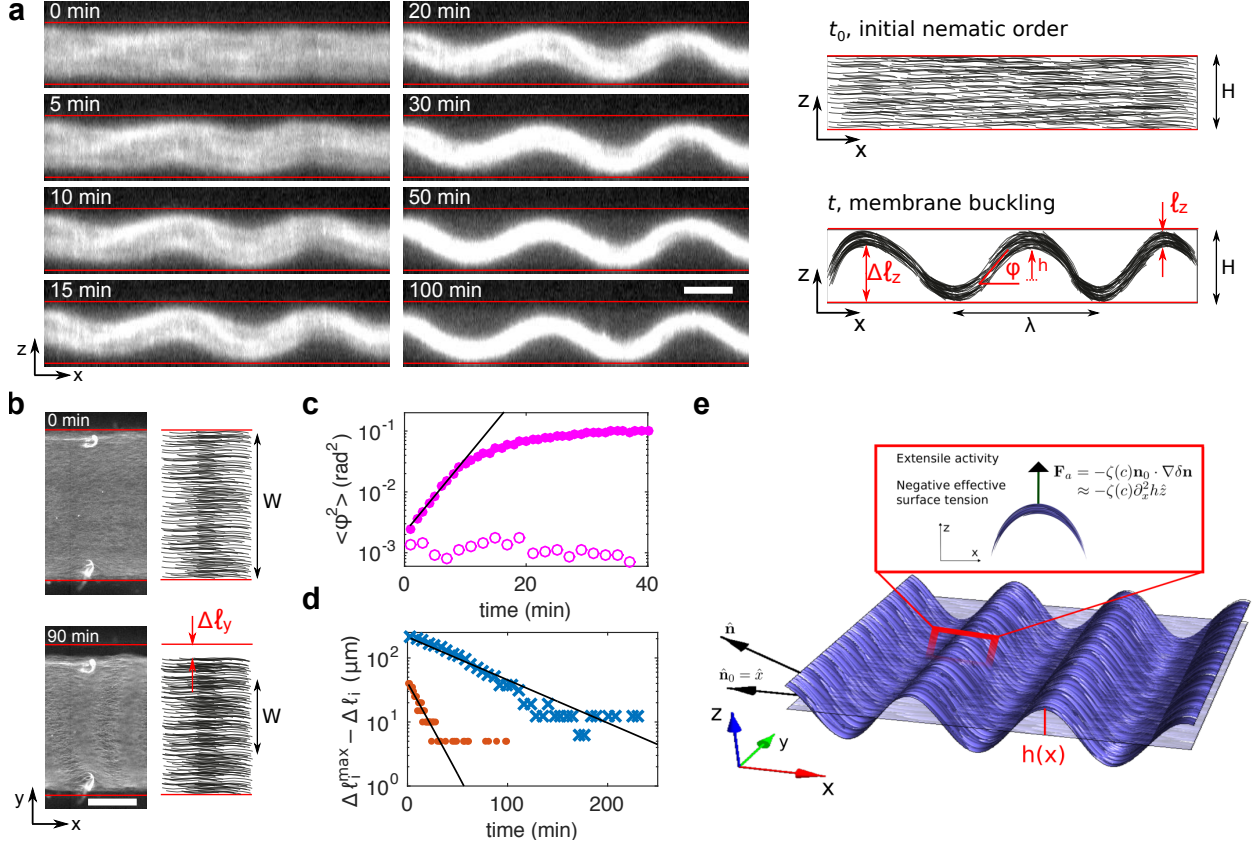


Figure 2: Dynamics and mechanism of the formation of a thin corrugated sheet at low motor concentration. **a** Time-lapse confocal fluorescence images of the active fluid in the xz plane (left) and sketch of the observations indicating the measured quantities Δl_z , ϕ , h , and l_z . Scale bar is $100 \mu\text{m}$. **b** Epifluorescence images of the fluid at $t = 0$ and 90 min (left) and sketch indicating the measured quantity Δl_y . Scale bar is $500 \mu\text{m}$. Red lines in panels a and b indicate channel walls. **c** Average of ϕ^2 along the x direction *vs.* time in the presence (filled disks) and in the absence of motors (empty circles). **d** Offset to the maximum contracted length along the z (red disks) and y (blue crosses) directions. Black lines in panels c and d are exponential fits. **e** Sketch of the mechanism for the active buckling of a thin membrane through the negative tension F_a proportional to the active stress $\zeta(c)$ and the Laplacian of the height $h(x)$ of the sheet above its fiducial plane. All data correspond to 0.5 nM motors except empty circles in panel c.

117 Buckling is active and contraction is passive

118 Passive gels of various compositions have been reported to form corrugations through Euler
 119 buckling when they are submitted either to an external contractile stress or to an extensile
 120 stress at constant length.^{24,25} To assess if this could explain our observations, we performed
 121 experiments that demonstrated, firstly, that buckling is principally an active process and,

122 secondly, that an Euler mechanism is not compatible with the data.

123 In the absence of motors buckling is undetectable in confocal images with the same
124 field of view in x as above (660 μm) (Figure 2c and Table S1), although it is weak but
125 detectable in images acquired over a wider field of view (Figure S3). In contrast, contraction
126 is similar both in passive and active fluids (Figure S3). The passive origin of contraction is
127 further supported by the fact that its amplitude is strongly dependent on the concentration
128 of depletion agent (Figure S4).

129 In passive fluids, depletion forces induce the condensation of microtubules into a dense
130 nematic fluid phase, which, in the absence of confinement, would relax to a highly anisotropic
131 tactoid droplet.³⁰ In the geometry of our experiments, this results in the formation of a quasi
132 2D sheet that elongates along the nematic axis x , thereby leading to Euler buckling in the
133 presence of boundaries. Indeed, a membrane with an excess area, which in this case arises
134 from the excess length $\Delta\ell_x = \ell_x - L$, where ℓ_x is the length of the membrane along x , will
135 have a buckled state beyond a critical $\Delta\ell_x^c$ that depends on H . Note that this mechanism
136 could in principle also explain active buckling if $\Delta\ell_x$ depends on the activity. However, this
137 sort of passive mechanism, reminiscent of the classic Euler buckling, is only possible if the
138 membrane had a fixed projected area, i.e. if it were confined in the x direction. On the
139 contrary, if active buckling were generated by local extensile forces exerted by the motors,
140 it would be independent of whether the fluid is constrained in length or not.

141 To test these two hypotheses, we performed experiments where one end of the fluid was
142 in contact with an aqueous solution and thus free to change length. In this configuration
143 (Figure 3) the active fluid buckled everywhere except on the tip close to the free boundary,
144 while the passive one did not buckle at all. We attribute the lack of buckling on the tip of
145 the active fluid to a gradient of microtubule concentration across the free boundary arising
146 during the preparation of the fluid (see SI Methods). These results suggest that, while the
147 excess area mechanism explains passive buckling, it cannot fully account for the buckling
148 of active films. We thus conclude, firstly, that passive and active buckling happen through

149 different mechanisms and, secondly, that in active fluids buckling is principally an active
 150 mechanism while contractions in y and z are mainly passive.

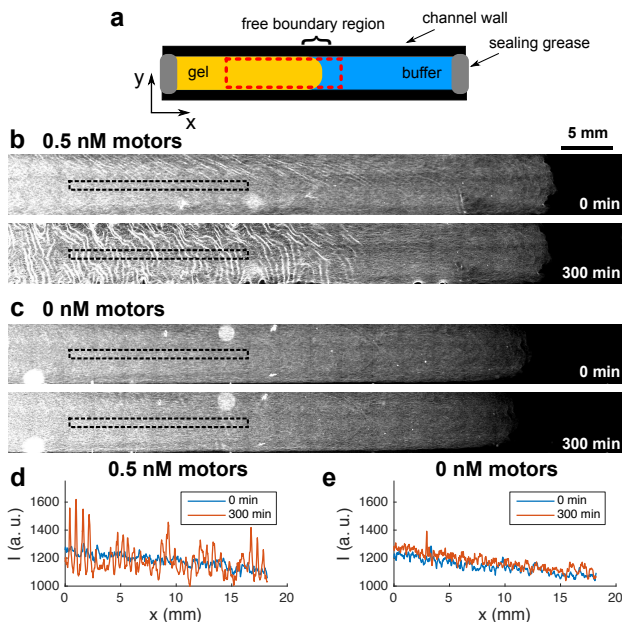


Figure 3: An active fluid buckles, in contrast with a passive one, in fluids with one free boundary. **a** Scheme of the experiment. The red dashed rectangle indicates the area where the images were recorded. Epifluorescence images of an active (**b**) and a passive (**c**) fluid at initial and final time. The black, dashed rectangles show the zones where the intensity profiles in **d** and **e** were extracted.

151 A hydrodynamic theory that predicts the wavenumber of the cor- 152 rugations

153 The behavior of active fluids, including those composed of microtubules and kinesins,^{4,22,31,32}
 154 has been successfully described with the hydrodynamic theory of liquid crystals supplemented
 155 with a stress term resulting from activity. We now demonstrate that this framework applied
 156 to a thin film that can buckle in the third dimension can provide an explanation and theoret-
 157 ical estimates of the wavenumber $q^* = 2\pi/\lambda$ and of the formation rate ω^* of the corrugated
 158 pattern (see Figure 2e and SI Section 2).

159 To do so, we consider the periodic undulation of the thin sheet made of microtubules and
 160 motors in the xz plane, supposing that passive forces have already collapsed the 3D fluid

161 into a thin 2D sheet. The nematic active fluid sheet has bending modulus K and its director
 162 $\hat{\mathbf{n}}$ is on average parallel to the x axis: $\hat{\mathbf{n}}_0 = \hat{x}$. The fluctuation of the membrane about a
 163 fiducial plane parallel to the xy plane (here, taken to be the mid-plane of the channel) is
 164 denoted by $h(x, y)$. The deflection of the director in the xz plane, $\delta\mathbf{n}_z$, leads to a buckling
 165 of the membrane in the z direction: $\delta\mathbf{n}_z \approx \partial_x h \hat{z}$. The passive elasticity of the nematic fluid
 166 $\propto (\nabla\mathbf{n})^2$ then yields a bending energy $\propto (K/2)(\partial_x^2 h)^2$ for the buckling of the thin sheet in
 167 the z direction. The standard active force^{5–9} is $-\zeta(c)\nabla \cdot (\mathbf{nn})$, where $\zeta(c) > 0$ is the strength
 168 of the extensile activity that is a function of motor concentration c . This leads to a force
 169 $\propto -\zeta(c)\partial_x^2 h \hat{z}$ that tends to destabilise the flat membrane and that is similar to an effective
 170 *negative* surface tension.³³ The interplay between the negative surface tension, arising from
 171 activity, and the stabilizing bending modulus, due to nematic elasticity, leads to the selection
 172 of a pattern with wavenumber

$$q^* \sim \sqrt{\zeta(c)/K}. \quad (1)$$

173 The pattern arises with a rate ω whose exact expression is provided in SI Section 2. Note
 174 that in the absence of confinement, we expect the pattern to be unstable.

175 The theory thus shows that an out-of-plane buckling instability compatible with our
 176 observations results from the interplay of active forcing $\zeta(c)$ and passive elastic restoring
 177 forces, K ; the same ingredients that in previous microtubule/kinesin active fluid provided
 178 dramatically different patterns.^{4,31,32,34,35} Here, the out-of-plane buckling of the active sheet
 179 precedes any planar pattern formation, in contrast to those experiments. In addition, the
 180 instability described here does not result in coherent or incoherent flow, of either the active
 181 or the embedding fluid, in contrast with theories describing 2D or 3D active fluids that do
 182 not form sheets.^{26,27,36}

183 This qualitative interpretation has two advantages. Firstly, it is parsimonious because a
 184 single feature, activity, explains the 3D out-of-plane buckling observed here and the 2D in-
 185 plane buckling^{4,32} and 3D chaotic flows²² observed previously in a similar system. Secondly,

186 it predicts that decreasing depletion forces precludes the formation of the thin sheet and
187 thus the emergence of out-of-plane buckling in favor of 3D chaotic flows. In the rest of
188 the paper we analyze these two questions in more detail. However, although hydrodynamic
189 theories, such as the one just described, provide an informative qualitative description of
190 the physics of active fluids, they feature phenomenological parameters, such as $\zeta(c)$ and K ,
191 that are difficult to measure experimentally. To our knowledge, the only quantitative test
192 of such theories in the kinesin-microtubule system was recently performed by Martinez-Prat
193 and colleagues,³² where they obtained $\zeta(c) \sim c^2$. Using their scaling, our semi-empirical
194 prediction reads

$$q^* \sim c/\sqrt{K}. \quad (2)$$

195 **Increasing the motor concentration linearly increases the wavenum-** 196 **ber of the corrugations and destabilizes the patterns**

197 To test the prediction $q^* \sim c$ we investigated the behavior of the fluid over a range of motor
198 concentrations c spanning more than two orders of magnitude (Figure 4 and Movie S2).
199 Below 0.5 nM motors, the fluid behaves as described in Figure 2: buckling in the xz plane
200 and contractions in the z and y directions. As c increases, between 1 and 2.5 nM motors,
201 buckling in the xz plane is initially observed and followed by buckling in the xy plane that
202 distorts the corrugated pattern without breaking it. Finally, between 5 and 50 nM motors,
203 buckling in the xz plane is still observed at early times but the pattern breaks into a 3D
204 active chaotic state similar to the one already reported in this active fluid^{4,22} (Movies S3
205 and S4). However, the velocity of this flow state is significantly lower in our case, possibly
206 because the solution is more viscous.

207 The transition to the chaotic state happens qualitatively through two processes: the
208 accumulated tension on the hills and valleys of the corrugations breaks the microtubule
209 bundles and the frozen fluid locally flows (Movie S2, 5 nM channel) or the dislocations

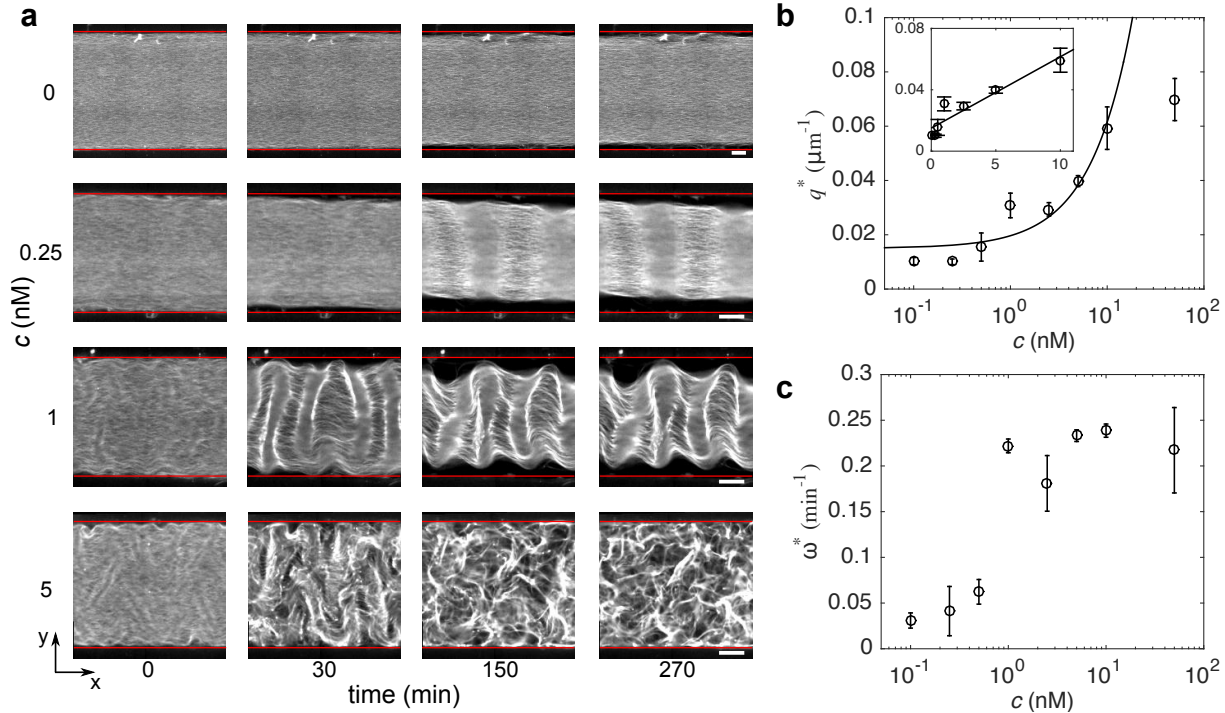


Figure 4: Dynamics, shape and stability of the patterns strongly depend on motor concentration. **a** Time-lapse epifluorescence images of fluids with different motor concentrations c . Red lines indicate channel walls. Scale bars are $200 \mu\text{m}$. **b** Wavenumber q^* of the corrugations *vs.* motor concentration. The inset is the lin-lin representation of the main plot and the line corresponds to a linear fit to the data in the range $c = 0.1 - 10$ nM with regression coefficient $r^2 = 0.9$. **c** Growth rate *vs.* motor concentration. Error bars indicate the standard deviation of a triplicate experiment where a single motor/filament mix was distributed into three different channels.

210 in the corrugations become motile leading to a shearing of the pattern and its consequent
 211 destruction (Movie S2, 10 nM channel). Note that, in our experiments, the chaotic state
 212 was never observed before the buckled state. However, if the characteristic time of active
 213 transport is much shorter than the time of passive contraction, one would observe only the
 214 spontaneous flow instability and would not observe the buckling instability (which happens
 215 in ref. 4). Nevertheless, first observing spontaneous flow instability and then the buckling
 216 instability is unlikely because the first one would destroy the nematic order that allows
 217 passive buckling.

218 Importantly, the measured wavenumber of the corrugations is in agreement with the
 219 predicted linear scaling (Figure 4b), in particular in the range $0.5 - 10$ nM. A linear fit

220 $q^* = a_1 + a_2 c$ of the data yields $a_1 = 5 \times 10^{-3} \mu\text{m}^{-1}$ and $a_2 = 1.4 \times 10^{-3} \mu\text{m}^{-1} \text{nM}^{-1}$, where
 221 the constant term a_1 results from the weak contribution of Euler buckling in the absence of
 222 motors. Indeed, activity controls the wavenumber only if the active wavenumber is larger
 223 than the one selected by passive Euler buckling, a crossover that in our experiments happens
 224 at $c = 0.5 \text{ nM}$.

225 The growth rate of the patterns, ω^* , increases slightly with c in the range $0.1 - 0.5 \text{ nM}$,
 226 then drastically between 0.5 and 1 nM , and saturates at higher c (Figure 4c and Fig-
 227 ure S5), resulting in ω^* also increasing and then saturating with q^* . For the hydrodynamics-
 228 dominated approximation, the theory predicts $\omega^* \sim q^3$ for $q^* H \gg 1$ and $\omega^* \sim q^6$ for
 229 $q^* H \ll 1$, while our experiments correspond to $q^* H = 1.3 - 4$. In the range $c = 0.1 - 0.5 \text{ nM}$,
 230 the data are compatible with the scaling $\omega^* \sim q^3$, although their precision does not allow to
 231 rule out other scaling laws (Figure S6).

232 Comparing the results of our out-of-plane instability with recent measurements of the in-
 233 plane buckling instability of a related system,³² we find similar wavenumbers ($1 - 7 \times 10^{-2} \mu\text{m}$
 234 in our case *vs.* $0.5 - 3 \times 10^{-2} \mu\text{m}$) but significantly slower dynamics ($1 - 4 \times 10^{-2} \text{ min}^{-1}$
 235 *vs.* $6 - 240 \text{ min}^{-1}$, respectively). In addition, topological defects seem to play no role in the
 236 emergence of our patterns, in contrast with what happens in 2D active nematic systems.^{21,34}
 237 We do observe dislocations in the corrugations that rarely move along the y axis, although
 238 they do so too slowly to play a significant role. In contrast, defects in the nematic field would
 239 create non-periodic buckled shapes in the z direction^{37,38} and we never observe this in our
 240 conditions.

241 **The thickness of the nematic fluid influences the corrugations**

242 To test the prediction $q^* \sim 1/\sqrt{K}$ we varied the thickness and the aspect ratio of the
 243 confinement of the active fluid at low motor concentration, with the hypotheses $K \sim \ell_z$ and
 244 $\ell_z \sim H$. Firstly, we measured ℓ_z and q^* for H in the range $70 - 540 \mu\text{m}$ and confirmed that
 245 the data are in agreement with $\ell_z \sim H$ and with $q^* \sim 1/\sqrt{\ell_z}$, with the exception of this last

246 scaling for the thinnest fluid (Figure 5). Secondly, reducing the aspect ratio of the channel
 247 section resulted in some portions of the fluid buckling in xz and others in the xy plane at
 248 $W/H = 4.6$ (Figure S8) and no preferential direction of buckling at $W/H = 1$ (Figure S9).
 249 In addition, in all the cases where both xy and xz buckling was observed, the wavenumbers
 250 in the two planes were in qualitative agreement with the aforementioned argument that
 251 essentially yields $q^* \sim 1/\sqrt{H} > q_{xy}^* \sim 1/\sqrt{W}$ when $H < W$ and $q^* = q_{xy}^*$ when $H = W$.

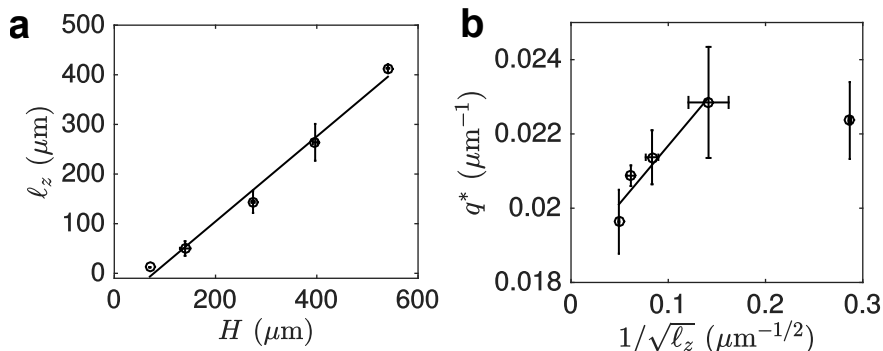


Figure 5: Increasing the thickness of the fluid reduces the wavenumber. **a** Final thickness ℓ_z vs. channel height H . **b** Wavenumber vs. $1/\ell_z^{1/2}$. Error bars indicate the standard deviation of a triplicate experiment where a single motor/filament mix was distributed into three different channels. Solid lines correspond to linear fits. 1 nM motors.

252 Another way to influence K is to change the microtubule concentration μ . Increasing μ
 253 in the range 0.5 – 2 mg/mL decreased q^* in agreement with the expectation that K should
 254 increase with μ . In contrast, at $\mu = 0.25$ mg/mL, global contraction, instead of corrugations,
 255 was observed, possibly because the initial nematic order was reduced (Figure S10).

256 **Strong attractive interactions between the microtubules are crucial** 257 **to form a corrugated sheet**

258 To the best of our knowledge, neither stable nor unstable out-of-plane buckling has been re-
 259 ported in nematic active fluids. We performed control experiments to determine which of the
 260 factors that differentiate our experiments from previously published 3D microtubule/kinesin
 261 nematics^{4,22,39} was responsible for the observed phenomenology: the type of motor or the
 262 length of the microtubules. We obtained both stable and unstable xz buckling with the

263 kinesin K401 used in previous reports⁴ (Figure S11). This means that, although the motor
264 K430 is not designed to form specific multimers, in contrast with K401, it forms non-specific
265 ones. Our efforts to eliminate these non-specific multimers by size exclusion chromatography
266 did not change the observed patterns (Figure S12), suggesting that these clusters either form
267 rapidly or do so in the working buffer.

268 In contrast with the nature of the motor, the length of the microtubules had a strong
269 impact on the observed structures. When, instead of 8 μm -long taxol-stabilized microtubules,
270 1.5 μm -long GMPCPP-stabilized ones were used, no contraction of the fluid was observed
271 along z or y , with or without motors, precluding the formation of a thin sheet that could
272 buckle out of plane (Figure S13). In this case, chaotic flow was observed at high activity, in
273 agreement with previous reports.⁴ These observations are consistent with the expected linear
274 dependence of the depletion free energy on filament length⁴⁰ which, in our geometry, makes
275 long microtubules condense into a thin sheet. To further test this hypothesis we reduced the
276 attractive force between negatively charged 8 μm -long microtubules by either lowering the
277 concentration of the depletion agent or the ionic strength of the buffer. In agreement with
278 this interpretation, neither fluid contraction, nor buckling in the xz plane, were apparent in
279 these conditions, although the fluid remained active (Figures S14 and S15).

280 **Comparison with other out-of-equilibrium membrane buckling**

281 The active buckling instability described here needs three ingredients: a thin film, nematic
282 order and extensile activity. We thus expect any system displaying these properties, such
283 as thin films that may be composed of living liquid crystals⁴¹ —which are suspensions of
284 living bacteria in an inert nematic solution— to buckle in a similar manner. Monolayers of
285 polarized living cells could potentially buckle in the same way, although so far only buckling
286 due to growth has been reported.⁴² Interestingly, a different type of active buckling has
287 recently been observed in a contractile isotropic film made of a crosslinked actin gel and
288 myosin.¹⁷ Despite their differences, for this contractile film to buckle, filaments also need to

289 form bundles, motors have to make aggregates and the observed thickness and wavelength
290 were of the same order of magnitude as those reported here.

291 Finally, we have described our system as an active fluid and not a gel to stress that
292 there are no permanent crosslinks between the microtubule filaments. This is supported by
293 the low concentration of motors relative to tubulin (1:1000 w/w at 1 nM motors) and by
294 the flows observed by us and others^{4,20-22,32} at high motor concentration. We believe that
295 the apparent contradiction of our observations with rheological measurements that reported
296 the presence of an effective cross-linking in pure microtubule solutions⁴³ could be explained,
297 either by the presence of microtubule bundles or by the longer timescale probed here (10^3 s
298 compared with 10^2 in ref. 43). Ultimately, precise rheological measurements of this type of
299 active fluids will provide a definite answer.

300 Conclusion

301 In summary, we demonstrate that in vitro active fluids can be designed to form static or
302 transient suspended sheets with periodic corrugated patterns of tunable wavelength. The
303 mechanism of pattern formation that we propose combines passive and active processes that
304 can be controlled physicochemically. Passive depletion forces, which depend on depletion
305 agent concentration, filament length and ionic strength, induce the spontaneous condensation
306 of a 3D nematic fluid into a thin 2D nematic sheet, and active stresses buckle the fluid sheet
307 out of plane to form corrugations with well-defined wavelength that can be controlled by
308 activity.

309 In addition, we use an active gel theory to demonstrate that the observed patterns re-
310 sult from an out of plane buckling instability induced by active extensile stresses along the
311 nematic axis of the fluid sheet, in contrast with in-plane buckling patterns that have been
312 observed in pre-stressed nematic fluids of either non-growing F-actin⁴⁴ and growing micro-
313 tubules⁴⁵ in the absence of motors. Our theory is appealing since it relies on the same essen-

314 tial physics that leads to 2D patterning and 2D and 3D spatio-temporal chaos. However, the
315 buckling instability that we report does not involve filament flows and therefore fundamen-
316 tally differs from both contractile instabilities in anisotropic active fluids and spontaneous
317 flow transitions in nematic active fluids that have been described theoretically,^{6,8,26,27,36,46}
318 and shown to be characterised by hydrodynamic flows and in-plane buckling of the director
319 field in the case of 2D systems. Such spontaneous flows have been observed in various active
320 matter systems,^{4,31,32,34,35,41,47–50} which in practice yield either chaotic or large scale coherent
321 flows, but so far no static spatial patterns. In contrast, our results show that active matter
322 can be shaped into long-lived static 3D patterns that can be tuned by activity, which may
323 open the way to the design of 3D biomimetic materials capable of morphogenesis.^{51,52}

324 **Material and Methods**

325 **Kinesin and microtubule preparation**

326 The K430 truncated kinesin-1 from *Rattus norvegicus*, containing a C-terminal SNAP tag,
327 was the homodimer version of the kinesin-1 described in ref. 28. K430 was expressed in *E.*
328 *coli*, purified using a Nickel affinity column thanks to a His-tag, dialyzed and flash frozen.
329 K401 was purified as described.⁵³ Tubulin and TRITC-labeled tubulin (Cytoskeleton) were
330 dissolved at 10 mg/mL in 1X PEM buffer (80 mM PIPES pH 6.8, 1 mM EGTA, 1 mM
331 MgSO₄) supplemented with 1 mM GTP, flash-frozen and stored at -80 °C. They were
332 polymerized in 1X PEM, 1 mM GTP, 10 % (w/v) glycerol and 5 mg/mL tubulin at (including
333 2.5 % fluorescent tubulin). Taxol-stabilized microtubules were incubated at 37 °C for 15 min
334 followed by the addition of 20 μ M paclitaxel, and stored at room temperature for few days.
335 GMPCPP-stabilized microtubules were polymerized in the presence of 0.5 mg/mL GMPCPP
336 (Jena Bioscience) from tubulin at 37 °C for 30 min and left at room temperature for 5 hours.
337 They were used within the same day. These procedures are described in more detail in SI
338 Section 1.

339 **Active mix**

340 The active mix consisted in 1X PEM buffer, 10 mM K-acetate, 10 mM KCl, 5 mM MgCl₂, 2
341 %(w/v) Pluronic F-127, 5 μg/mL creatine kinase, 20 mM creatine phosphate, 20 μM taxol,
342 2 mM ATP, 1 mg/mL BSA, 1 mM trolox, 20 mM D-glucose, 3 mM DTT, 150 μg/mL glucose
343 oxidase, 25 μg/mL catalase and 0.5 mg/mL taxol-stabilized microtubules.

344 **Channel assembly**

345 Channels were assembled using a microscope glass slide (26 x 75 x 1 mm) and a coverslip
346 (22 x 50 x 0.17 mm) separated by strips of Parafilm cut with a Graphtec Cutting Plotter
347 CE6000-40. Both microscope glass slides and coverlips were passivated using an acrylamide
348 brush.⁵⁴ The active mix was filled in the flow cell (22 x 1.5 x 0.130 mm) by capillarity and
349 sealed with vacuum grease.

350 **Imaging**

351 Epifluorescence images were obtained with a Zeiss Observer 7 automated microscope equipped
352 with a Hamamatsu C9100-02 camera, a 10X objective, a motorized stage and controlled with
353 MicroManager 1.4. Images were recorded automatically every 3 min using an excitation at
354 550 nm with a CoolLED pE2. Confocal images were obtained with a Leica TCS SP5 II
355 confocal microscope with a 25x water-immersion objective or a X-Light V2 Spinning Disk
356 Confocal system mounted on an upright Nikon Eclipse 80i microscope with a 10x objective.
357 Images were recorded automatically every 1 to 10 min.

358 **Image analysis**

359 Fluorescent images were binarized to obtain $\Delta\ell_z$ and $\Delta\ell_y$. To measure ϕ the binarized
360 xz confocal cross-sections were averaged over x , smoothed along x by applying a moving
361 average filter with a 30-pixel window, that was then differentiated. ϕ was the arctangent of

362 this derivative.

363 **Note added in proof**

364 During the revision process a similar observation was reported in the arXiv.⁵⁵

365 **Acknowledgements**

366 K. Furuta for providing the expression plasmids coding for the K430 kinesin, Z. Gueroui
367 for a kind gift of the K401 plasmid, F. Lam from the microscopy platform at IBPS and
368 L.L. Pontani for providing access to a spinning disk microscope, T. Surrey for insightful
369 discussions and C. del Junco and Y. Vyborna for comments on the manuscript. This work
370 has been funded by the European Research Council (ERC) under the European's Union
371 Horizon 2020 programme (grant No 770940, A.E.-T.) and by the Ville de Paris Emergences
372 programme (Morphoart, A.E.-T.). The data that support the findings of this study are
373 available from the corresponding author upon reasonable request.

374 **References**

- 375 (1) Cavagna, A.; Cimarelli, A.; Giardina, I.; Parisi, G.; Santagati, R.; Stefanini, F.;
376 Viale, M. Scale-free correlations in starling flocks. *Proceedings of the National Academy
377 of Sciences* **2010**, *107*, 11865–11870.
- 378 (2) Dombrowski, C.; Cisneros, L.; Chatkaew, S.; Goldstein, R. E.; Kessler, J. O. Self-
379 Concentration and Large-Scale Coherence in Bacterial Dynamics. *Phys. Rev. Lett.*
380 **2004**, *93*, 098103.
- 381 (3) Nédélec, F. J.; Surrey, T.; Maggs, A. C.; Leibler, S. Self-organization of microtubules
382 and motors. *Nature* **1997**, *389*, 305–308.

- 383 (4) Sanchez, T.; Chen, D. T.; DeCamp, S. J.; Heymann, M.; Dogic, Z. Spontaneous motion
384 in hierarchically assembled active matter. *Nature* **2012**, *491*, 431–4.
- 385 (5) Toner, J.; Tu, Y.; Ramaswamy, S. Hydrodynamics and phases of flocks. *Annals of*
386 *Physics* **2005**, *318*, 170 – 244.
- 387 (6) Jülicher, F.; Kruse, K.; Prost, J.; Joanny, J.-F. Active behavior of the Cytoskeleton.
388 *Physics Reports* **2007**, *449*, 3 – 28.
- 389 (7) Ramaswamy, S. The Mechanics and Statistics of Active Matter. *Annual Review of*
390 *Condensed Matter Physics* **2010**, *1*, 323–345.
- 391 (8) Marchetti, M. C.; Joanny, J. F.; Ramaswamy, S.; Liverpool, T. B.; Prost, J.; Rao, M.;
392 Simha, R. A. Hydrodynamics of soft active matter. *Reviews of Modern Physics* **2013**,
393 *85*, 1143–1189.
- 394 (9) Prost, J.; Julicher, F.; Joanny, J. F. Active gel physics. *Nat Phys* **2015**, *11*, 111–117.
- 395 (10) Dogterom, M.; Surrey, T. Microtubule organization in vitro. *Current Opinion in Cell*
396 *Biology* **2013**, *25*, 23–29.
- 397 (11) Blanchoin, L.; Boujemaa-Paterski, R.; Sykes, C.; Plastino, J. Actin Dynamics, Archi-
398 tecture, and Mechanics in Cell Motility. *Physiological Reviews* **2014**, *94*, 235–263.
- 399 (12) Bendix, P. M.; Koenderink, G. H.; Cuvelier, D.; Dogic, Z.; Koeleman, B. N.;
400 Briehar, W. M.; Field, C. M.; Mahadevan, L.; Weitz, D. A. A quantitative analysis
401 of contractility in active cytoskeletal protein networks. *Biophysical journal* **2008**, *94*,
402 3126–3136.
- 403 (13) Needleman, D.; Dogic, Z. Active matter at the interface between materials science and
404 cell biology. *Nature reviews Materials* **2017**, *2*, 17048–17048.

- 405 (14) Alvarado, J.; Sheinman, M.; Sharma, A.; MacKintosh, F. C.; Koenderink, G. H. Molec-
406 ular motors robustly drive active gels to a critically connected state. *Nature Physics*
407 **2013**, *9*, 591.
- 408 (15) Foster, P. J.; Fürthauer, S.; Shelley, M. J.; Needleman, D. J. Active contraction of
409 microtubule networks. *eLife* **2015**, *4*, e10837.
- 410 (16) Torisawa, T.; Taniguchi, D.; Ishihara, S.; Oiwa, K. Spontaneous Formation of a Globally
411 Connected Contractile Network in a Microtubule-Motor System. *Biophysical journal*
412 **2016**, *111*, 373–385.
- 413 (17) Ideses, Y.; Erukhimovitch, V.; Brand, R.; Jourdain, D.; Hernandez, J. S.; Gabi-
414 net, U. R.; Safran, S. A.; Kruse, K.; Bernheim-Groswasser, A. Spontaneous buckling of
415 contractile poroelastic actomyosin sheets. *Nature Communications* **2018**, *9*, 2461.
- 416 (18) Schaller, V.; Weber, C.; Semmrich, C.; Frey, E.; Bausch, A. R. Polar patterns of driven
417 filaments. *Nature* **2010**, *467*, 73.
- 418 (19) Sumino, Y.; Nagai, K. H.; Shitaka, Y.; Tanaka, D.; Yoshikawa, K.; Chaté, H.; Oiwa, K.
419 Large-scale vortex lattice emerging from collectively moving microtubules. *Nature*
420 **2012**, *483*, 448.
- 421 (20) Doostmohammadi, A.; Ignés-Mullol, J.; Yeomans, J. M.; Sagués, F. Active nematics.
422 *Nature Communications* **2018**, *9*, 3246.
- 423 (21) Kumar, N.; Zhang, R.; de Pablo, J. J.; Gardel, M. L. Tunable structure and dynamics
424 of active liquid crystals. *Science Advances* **2018**, *4*.
- 425 (22) Wu, K.-T.; Hishamunda, J. B.; Chen, D. T. N.; DeCamp, S. J.; Chang, Y.-W.;
426 Fernández-Nieves, A.; Fraden, S.; Dogic, Z. Transition from turbulent to coherent flows
427 in confined three-dimensional active fluids. *Science* **2017**, *355*.

- 428 (23) Roostalu, J.; Rickman, J.; Thomas, C.; Nédélec, F.; Surrey, T. Determinants of Polar
429 versus Nematic Organization in Networks of Dynamic Microtubules and Mitotic Motors.
430 *Cell* **2018**, *175*, 796–808.e14.
- 431 (24) Matsuo, E. S.; Tanaka, T. Patterns in shrinking gels. *Nature* **1992**, *358*, 482–485.
- 432 (25) Islam, M. F.; Alsayed, A. M.; Dogic, Z.; Zhang, J.; Lubensky, T. C.; Yodh, A. G.
433 Nematic Nanotube Gels. *Phys. Rev. Lett.* **2004**, *92*, 088303.
- 434 (26) Kruse, K.; Joanny, J.-F.; Jülicher, F.; Prost, J.; Sekimoto, K. Asters, vortices, and ro-
435 tating spirals in active gels of polar filaments. *Physical review letters* **2004**, *92*, 078101.
- 436 (27) Voituriez, R.; Joanny, J. F.; Prost, J. Spontaneous flow transition in active polar gels.
437 *Europhysics Letters (EPL)* **2005**, *70*, 404–410.
- 438 (28) Furuta, K.; Furuta, A.; Toyoshima, Y. Y.; Amino, M.; Oiwa, K.; Kojima, H. Measuring
439 collective transport by defined numbers of processive and nonprocessive kinesin motors.
440 *Proceedings of the National Academy of Sciences* **2013**, *110*, 501–506.
- 441 (29) de Gennes, P. G.; Prost, J. *The physics of liquid crystals (second edition)*; Oxford
442 university press, 1993.
- 443 (30) Kaznacheev, A. V.; Bogdanov, M. M.; Taraskin, S. A. The nature of prolate shape of
444 tactoids in lyotropic inorganic liquid crystals. *J. Exp. Theo. Phys.* **2002**, *95*, 57–63.
- 445 (31) Keber, F. C.; Loiseau, E.; Sanchez, T.; DeCamp, S. J.; Giomi, L.; Bowick, M. J.;
446 Marchetti, M. C.; Dogic, Z.; Bausch, A. R. Topology and dynamics of active nematic
447 vesicles. *Science* **2014**, *345*, 1135–1139.
- 448 (32) Martínez-Prat, B.; Ignés-Mullol, J.; Casademunt, J.; Sagués, F. Selection mechanism
449 at the onset of active turbulence. *Nature Physics* **2019**,
- 450 (33) Maitra, A.; Srivastava, P.; Rao, M.; Ramaswamy, S. Activating Membranes. *Phys. Rev.*
451 *Lett.* **2014**, *112*, 258101.

- 452 (34) DeCamp, S. J.; Redner, G. S.; Baskaran, A.; Hagan, M. F.; Dogic, Z. Orientational
453 order of motile defects in active nematics. *Nature Materials* **2015**, *14*, 1110 EP –.
- 454 (35) Opathalage, A.; Norton, M. M.; Juniper, M. P. N.; Langeslay, B.; Aghvami, S. A.;
455 Fraden, S.; Dogic, Z. Self-organized dynamics and the transition to turbulence of con-
456 fined active nematics. *Proceedings of the National Academy of Sciences* **2019**, *116*,
457 4788–4797.
- 458 (36) Edwards, S. A.; Yeomans, J. M. Spontaneous flow states in active nematics: A unified
459 picture. *EPL (Europhysics Letters)* **2009**, *85*, 18008.
- 460 (37) Seung, H. S.; Nelson, D. R. Defects in flexible membranes with crystalline order. *Phys.*
461 *Rev. A* **1988**, *38*, 1005–1018.
- 462 (38) Frank, J. R.; Kardar, M. Defects in nematic membranes can buckle into pseudospheres.
463 *Phys. Rev. E* **2008**, *77*, 041705.
- 464 (39) Henkin, G.; DeCamp, S. J.; Chen, D. T. N.; Sanchez, T.; Dogic, Z. Tunable dynamics of
465 microtubule-based active isotropic gels. *Philosophical Transactions of the Royal Society*
466 *A: Mathematical, Physical and Engineering Sciences* **2014**, *372*.
- 467 (40) Braun, M.; Lansky, Z.; Hilitski, F.; Dogic, Z.; Diez, S. Entropic forces drive contraction
468 of cytoskeletal networks. *BioEssays* **2016**, *38*, 474–481.
- 469 (41) Zhou, S.; Sokolov, A.; Lavrentovich, O. D.; Aranson, I. S. Living liquid crystals. *Pro-*
470 *ceedings of the National Academy of Sciences* **2014**, *111*, 1265–1270.
- 471 (42) Nelson, M. R.; Howard, D.; Jensen, O. E.; King, J. R.; Rose, F. R. A. J.; Wa-
472 ters, S. L. Growth-induced buckling of an epithelial layer. *Biomechanics and Modeling*
473 *in Mechanobiology* **2011**, *10*, 883–900.
- 474 (43) Lin, Y.-C.; Koenderink, G. H.; MacKintosh, F. C.; Weitz, D. A. Viscoelastic Properties
475 of Microtubule Networks. *Macromolecules* **2007**, *40*, 7714–7720.

- 476 (44) Gentry, B.; Smith, D.; Käs, J. Buckling-induced zebra stripe patterns in nematic F-
477 actin. *Physical Review E* **2009**, *79*, 031916.
- 478 (45) Liu, Y.; Guo, Y.; Valles, J. M.; Tang, J. X. Microtubule bundling and nested buckling
479 drive stripe formation in polymerizing tubulin solutions. *Proceedings of the National*
480 *Academy of Sciences* **2006**, *103*, 10654–10659.
- 481 (46) Bois, J. S.; Jülicher, F.; Grill, S. W. Pattern Formation in Active Fluids. *Physical*
482 *Review Letters* **2011**, *106*, 028103.
- 483 (47) Wensink, H. H.; Dunkel, J.; Heidenreich, S.; Drescher, K.; Goldstein, R. E.; Löwen, H.;
484 Yeomans, J. M. Meso-scale turbulence in living fluids. *Proceedings of the National*
485 *Academy of Sciences* **2012**, *109*, 14308–14313.
- 486 (48) Kumar, A.; Maitra, A.; Sumit, M.; Ramaswamy, S.; Shivashankar, G. V. Actomyosin
487 contractility rotates the cell nucleus. *Scientific Reports* **2014**, *4*, 3781 EP –.
- 488 (49) Duclos, G.; Erenkämper, C.; Joanny, J.-F.; Silberzan, P. Topological defects in confined
489 populations of spindle-shaped cells. *Nature Physics* **2016**, *13*, 58 EP –.
- 490 (50) Duclos, G.; Blanch-Mercader, C.; Yashunsky, V.; Salbreux, G.; Joanny, J.-F.; Prost, J.;
491 Silberzan, P. Spontaneous shear flow in confined cellular nematics. *Nature Physics*
492 **2018**, *14*, 728–732.
- 493 (51) Zadorin, A. S.; Rondelez, Y.; Gines, G.; Dilhas, V.; Urtel, G.; Zambrano, A.; Galas, J.-
494 C.; Estevez-Torres, A. Synthesis and materialization of a reaction–diffusion French flag
495 pattern. *Nature Chemistry* **2017**, *9*, 990.
- 496 (52) Furuta, K.; Furuta, A. Re-engineering of protein motors to understand mechanisms bi-
497 asing random motion and generating collective dynamics. *Current Opinion in Biotech-*
498 *nology* **2018**, *51*, 39–46.

- 499 (53) Subramanian, R.; Gelles, J. Two distinct modes of processive kinesin movement in
500 mixtures of ATP and AMP-PNP. *The Journal of general physiology* **2007**, *130*, 445–
501 455.
- 502 (54) Sanchez, T.; Dogic, Z. *Methods in Enzymology*; Elsevier, 2013; Vol. 524; pp 205–224.
- 503 (55) Strübing, T.; Khosravanizadeh, A.; Vilfan, A.; Bodenschatz, E.; Golestanian, R.;
504 Guido, I. Wrinkling instability in 3D active nematics. *arXiv:1908.10974*